ECCOMAS Congress 2016
VII European Congress on Computational Methods in Applied Sciences and Engineering
M. Papadrakakis, V. Papadopoulos, G. Stefanou, V. Plevris (eds.)
Crete Island, Greece, 5–10 June 2016

EFFICIENCY OF DAMAGE-PLASTICITY MODELS IN CAPTURING COMPACTION-EXPANSION TRANSITION OF CONCRETE UNDER DIFFERENT COMPRESSION LOADING CONDITIONS

Reza Mousavi[1], Masoud D. Champiri[2], and Kaspar J. Willam[3]

[1]University of Houston, Department of Civil Engineering
Houston , TX
e-mail: mmousavi@uh.edu

[2] University of Houston, Department of Civil Engineering
Houston , TX
e-mail: mdehghanichampiri@uh.edu

[3] University of Houston, Department of Civil Engineering
Houston , TX
e-mail: kwillam@central.uh.edu

Keywords: concrete, damage, plasticity, dilation, multiaxial behavior

Abstract. *The pre- and post-peak performance features of two widely used damage-plasticity constitutive formulations are assessed for modeling the multiaxial response behavior of pressure sensitive quasi-brittle materials such as concrete. Two benchmark problems have been solved using commercial software packages; ABAQUS which implements the two invariant Lee-Fenves damaged plasticity formulation as its main feature for concrete has been used along with LS-DYNA which is using Duvaut-Lion damage and plasticity model, a three invariant formulation. In order to have consistent results, the parameter identification and calibration for both models has been performed and response of both models has been compared to each other under uniaxial tension and compression. The two benchmark problem are triaxial compression CTC and triaxial tension CTE. The aim of this study is to observe the difference between two well-known material models in capturing the compaction to extension regime in the yielded material. The difference between the response of each material model and also the efficiency of input parameters in controlling of this transition has been studied in this paper. Based on these failure diagnostics, the main shortcomings of each formulation are discussed and possible enhancements and remedies are proposed for the pre- and post-peak feature.*

1 introduction

The usage of commercial packages is world wide and they have many applications in the he computational mechanics. Between these packages, for sure, ABAQUS [1] and LS-DYNA [2] have more interest than others. Since different material models are developed in these packages for same material like concrete, it is necessary to compare them together and see how the user can get similar results with implementing some parameters. This can help them to use material models widely and in different cases and situations.
Many concrete material models have been developed and implemented in these packages. Damage and plasticity are two important features where users are looking for them in order to use concrete material models. In ABAQUS, concrete damaged plasticity model (CDP) [3, 4], is widely used among researchers [5–8]. The constitutive formulation of this material model is reviewed in the following sections. Many concrete material models are available in LS-DYNA where they consider damage and plasticity [9]. Karagozian and Case model (concrete damage model, MAT-72) [10], the Riedel-Hiermaier-Thoma model (RHT, MAT-272) [11, 12], the Brannon-Fossum model (BF1) [13], and Continuous surface cap model (CSCM, MAT-159) [14] are some of those. Among them, MAT-159 has many applications in the literature [15, 16], because this material uses two parameters including uniaxial compressive strength and maximum size of aggregate in the simplest version for concrete structures, while other materials need many inputs. This material model uses the Duvaut-Lions formulation [17] and its constitutive model will be addressed in the section 3 of this paper. As a result, these two material models in ABAQUS and LS-DYNA have been selected and their behavior is compared together. It is tried to find a way to make their behavior closer to each other with implementing a parameter study. For this, their behavior is compared in uniaxial compression test, uniaxial tension test. Later on, with adopted parameters, the behavior of these material models is investigated in case of triaxial compression test (CTC), triaxial extension test (CTE) and bi-axial compression test. These tests can be also done experimentally as Kupfer et.al [18]. In order to compare the with the experimental results, one option to observe a more general localized behavior of concrete under different levels of confinement, full field measurment techniques like digital image correlation (DIC) method can be utilized [19–22]. A remarkable feature that can be pointed out about post processing of digital image correlation system is their feasibility in being implemented in expert systems. Champiri et al [23, 24]developed some expert systems for concrete structures and structural health monitoring with developing a fuzzy method. The parameter study is conducted in section 4 and the most efficient parameters are selected for performing different tests. Also it is noted that each material model has some deficiencies as well as some advantages in some points. Some concluding remarks are investigated in section 5.

2 Concrete Damaged Plasticity model

In this model, the admissible stress state has the condition of [4]:

$$F(\sigma, f_t, f_c) \leq 0 \tag{1}$$

In which, $f_t = f_t(\kappa_t), \quad f_c = f_c(\kappa_c)$ are tensile and comressive uniaxial strengths which are written as functions of damage parameter respectively. By rearranging uniaxial strength values as function of scalar degradation, the relation between the effective strength and strength is as follow:

$$f_t = (1 - D_t(\kappa_t))\bar{f}_t(\kappa_t), \quad f_c = (1 - D_c(\kappa_c))\bar{f}_c(\kappa_c) \tag{2}$$

The damage variable in CDP model is defined as scalar quantity which is different in compression and tension [3]. the uniaxial version of this parameter is defined as follow:

$$\kappa_\chi = \frac{\int_0^{\varepsilon^p} \sigma_\chi(\varepsilon^p) d\varepsilon^p}{\int_0^{\infty} \sigma_\chi(\varepsilon^p) d\varepsilon^p} \tag{3}$$

Here, $g_\chi = \int_0^{\infty} \sigma_\chi(\varepsilon^p) d\varepsilon^p$ is called dissipated energy density per unit volume. This quantity has been obtained by regularization of fracture energy in tensile and compressive state (G_χ) with respect to characteristic element size (l_χ) as $g_\chi = G_\chi / l_\chi$. the relation between stress an strain is written as follow:

$$\sigma_\chi = f_{\chi 0}((1 + a_\chi)e^{-b_\chi \varepsilon^p} - a_\chi e^{-2b_\chi \varepsilon^p}) \tag{4}$$

In which, a_χ, b_χ are constants. The relation between degradation and plastic strain is written as:

$$1 - D_\chi = e^{-d_\chi \varepsilon^p} \tag{5}$$

By taking into account degradation, the effective stress is calculated as follow:

$$\bar{\sigma}_\chi = f_{\chi 0}((1 + a_\chi)(e^{-b\varepsilon^p})^{1 - \frac{d_\chi}{b_\chi}} - a_\chi (e^{-b_\chi \varepsilon^p})^{2 - \frac{d_\chi}{b_\chi}}) \tag{6}$$

By combining eq.(4),(6) with eq.(5), we have:

$$g_\chi = \frac{f_{\chi 0}}{b_\chi}\Big(1 + \frac{a_\chi}{2}\Big) \tag{7}$$

$$\sigma_\chi = \frac{f_{\chi 0}}{a_\chi}\Big((1 + a_\chi)\sqrt{\phi_\chi(\kappa_\chi)} - \phi_\chi(\kappa_\chi)\Big) \tag{8}$$

By eq. (8) and (3), the damage evolution law in the uniaxial test is obtained by:

$$\dot{\kappa}_\chi = \frac{1}{g_\chi} f_\chi(\kappa_\chi)\dot{\varepsilon}^p \tag{9}$$

For the case of compressive stress, a damage value of κ_c' has been assumed when compressive stress is at its peak which gives corresponding degradation value of D_c as an input parameter for the material model which will be discussed in following. By putting this damage value into eq. ref$eq_stress2$, we will have following:

$$\sqrt{\phi(\kappa_c')} = \frac{1 + a_c}{2} \rightarrow D_c = 1 - \Big(\frac{1}{a_c}\Big(1 + a_c - \frac{1 + a_c}{2}\Big)\Big)^{\frac{d_c}{b_c}} \tag{10}$$

Since D_c is measured from experiment, we can obtain d_c/b_c by equation:

$$\frac{d_c}{b_c} = \frac{\log(1 - D_c)}{\log\left(\frac{1+a_c}{2a_c}\right)} \tag{11}$$

In the case of tensile loading, since the stress diagram is descending from the beginning of plastification, a tensile degradation value D_t will be considered at the point where stress value is half of the value of tensile strength $(\sigma_t = f_{t0}/2))$. for this case, we have:

$$\sqrt{\phi(\kappa_t)} = \frac{1 + a_t + \sqrt{1 + a_t^2}}{2} \tag{12}$$

$$\frac{d_t}{b_t} = \frac{\log(1 - D_t)}{\log((1 + a_t) - \sqrt{1 + a_t^2}) - \log 2a_t} \tag{13}$$

3 Material 159

The yield function for this material model reads as [14]:

$$\phi_{159}(I_1, J_2, J_3, \kappa) = J_2 - \Re^2 F_f^2 F_c \tag{14}$$

in which,$F_f(I_1), F_c(I_1, \kappa), \Re(J_2, J_3)$ are functions which are taking into shear surface, cap region and Rubin scaling factor [25], respectively.

$$F_f(I_1) = \alpha - \lambda e^{-\beta_0 I_1} + \theta I_1 \tag{15}$$

$$F_c(I_1, \kappa) = \begin{cases} 1 - \frac{(I_1-\kappa)^2}{(X-\kappa)^2} & : I_1 \geq \kappa_0 \\ 1 & : otherwise \end{cases} \tag{16}$$

$$\Re(J_2, J_3) = \frac{-b_1 + \sqrt{b_1^2 - 4b_1 b_0}}{2b_2} \tag{17}$$

$$L(\kappa) = \begin{cases} \kappa & : \kappa > \kappa_0 \\ \kappa_0 & : \kappa \leq \kappa_0 \end{cases} \tag{18}$$

$$X(\kappa) = L(\kappa) + R_0 F_f(L(\kappa)) \tag{19}$$

By Definition:

$$b_0 = -\frac{3 + b - a^2}{4} \tag{20a}$$

$$b_1 = a(\cos\beta - a\sin\beta) \tag{20b}$$

$$b_2 = (\cos\beta - a\sin\beta)^2 + b\sin^2\beta \tag{20c}$$

$$b = (2Q_1 + a)^2 - 3$$

$$a = \frac{-a_1 + \sqrt{a_1^2 - 4a_2 a_0}}{2a_2} \tag{20d}$$

$$a_0 = 2Q_1^2(Q_2 - 1) \tag{20e}$$

$$a_1 = \sqrt{3}Q_2 + 2Q_1(Q_2 - 1) \tag{20f}$$

$$a_2 = Q_2 \tag{20g}$$

$$\sin 3\hat{\beta} = \frac{3\sqrt{3}J_3}{2J_2^{3/2}} \tag{20h}$$

Q_1 and Q_2 are the parameters which determine the yield surface parameters that we want to fit. As a generalized form:

$$Q_1 = \alpha_1 - \lambda_1 e^{-\beta_1 I_1} + \theta_1 I_1 \tag{21a}$$

$$Q_2 = \alpha_2 - \lambda_2 e^{-\beta_2 I_1} + \theta_2 I_1 \tag{21b}$$

In formulation for material 159, the softening is modeled using damage formulation for tensile and in the case of compression with moderate confinement. It means that the softening is not activated unless damage formulation is activated. Unlike CDP model, in which, damage parameter had indirect effect on softening behavior, in material 159, softening behavior and stiffness degradation (modulus reduction) are in direct correlation with each other. The scalar damage parameter is categorized into two different categories: brittle damage, which happens

when stress state is tensile and ductile damage, in which, the stress state is compressive. The ductile and brittle damage evolution functions, are as follow:

$$d(\tau_b) = \frac{0.999}{D}\Big(\frac{1+D}{1+De^{-C(\tau_b - r_{0b})}} - 1\Big) \tag{22}$$

$$d(\tau_d) = \frac{d_{max}}{B}\Big(\frac{1+B}{1+Be^{-A(\tau_d - r_{0d})}} - 1\Big) \tag{23}$$

In which, d is scalar damage parameter, τ_b, τ_d are strain energy corresponding to current strain state and r_{0b}, r_{0d} are initial damage threshold for brittle and ductile damage,respectively.
$A,\ B,\ C,\ D$ are softening parameters for compression (A, B) and tension (C, D), respectively. d_{max} is maximum damage parameter which can be defined. (recommended to take $d_{max} < 1$ and is usually taken $d_{max} > 0.99$).
The fracture energy is calculated from the following:

$$G_f = \int_{u_0}^{\infty} (1-d) f' dx \tag{24}$$

in which, u_0 is displacement corresponding to the peak strength value.
By putting eq. (22) into eq. (24), relationship between fracture energy and softening parameters for brittle damage is calculated as follow:

$$G_f = r_{0b} L\Big(\frac{1+D}{CD}\Big) \tag{25}$$

based on eq. (25), a parameter reduction can be done by eliminating parameter C from the brittle damage evolution eq. (22):

$$C = r_{0b} L\Big(\frac{1+D}{G_f D}\Big)\log(1+D) \tag{26}$$

parameter reduction for ductile damage is obtained from following equation:

$$G_f = 2r_{0d} L\Big(\frac{1+B}{AB}\Big)\log(1+B) + 2L\Big(\frac{1+B}{A^2}\Big)\int_0^{\infty} \frac{ye^{-y}dy}{1+Be^{-y}} \tag{27}$$

In which, $y = -A(\sqrt{u} - \sqrt{u_0})\sqrt{\frac{f'}{L}}$. The integral for equation above doesn't have closed form solution. It is calculated numerically and the value is shown as $dilog$. By re-arranging eq. (27), the parameter A is obtained as following:

$$A = \frac{-b + \sqrt{b^2 - 4c}}{2} \tag{28}$$

$$b = \frac{-2(1+B)\log(1+B)Lr_{0d}}{BG_f} \tag{29}$$

$$c = \frac{-2L(1+B)dilog}{G_f} \tag{30}$$

Based on equations above after parameter reduction, the parameter that determines compressive behavior of concrete in the post peak regime, in addition to compressive fracture energy is B. Similarly, The parameter which shapes the post peak behavior of concrete under tensile loading condition, is D along with tensile fracture energy. The discussion about these parameters and values of each parameter are shown in the next section.

4 Parameter Evaluation for material models

Since finding analytical equivalence of each parameter is a very complicated task and needs a big amount of energy and time, here, the CDP parameters are calculated based on their numerical counter parts as used in material 159. The set of inputs for material are as shown in table 1. The set of parameters which are necessary to define a stress-strain curve and its compatible damage evolution law is mentioned in table 2.The material model has been assigned to a single cube element with displacement boundary conditions at one top side and symmetric boundary conditions in two perpendicular sides. the roller supports restraining bottom of the element from moving along load direction has been applied to the model. The analysis has been implemented in both packages in the case of uniaxial compression and tension and the results are compared in terms of stress vs strain, stress vs volumetric strain and damage evolution with respect to plastic strain as shown in figures 1 - 6

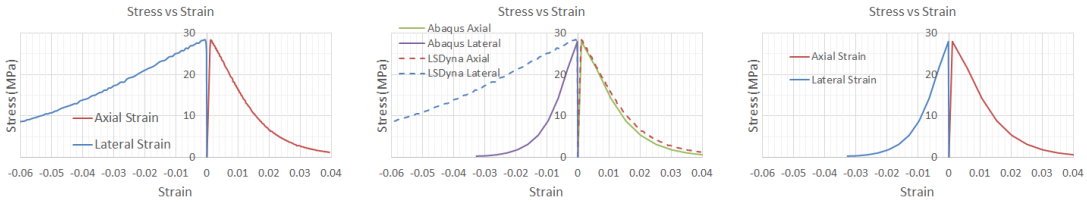

Figure 1: Uniaxial compression results of LS-DYNA (Left), Abaqus (Right), and their stress vs strain comparison (Middle).

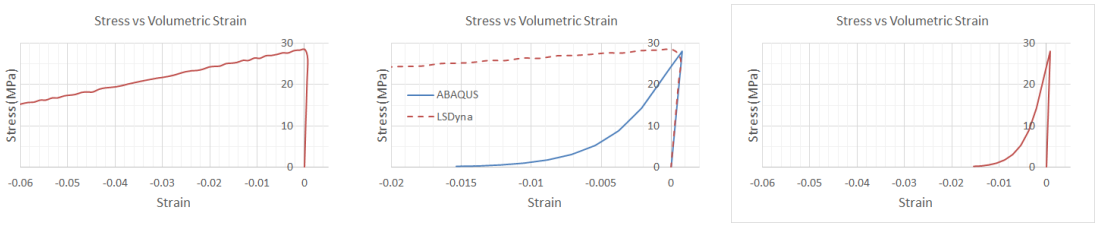

Figure 2: Compaction to extension behavior as of LS-DYNA (Left), Abaqus (Right) and their comparison (Middle).

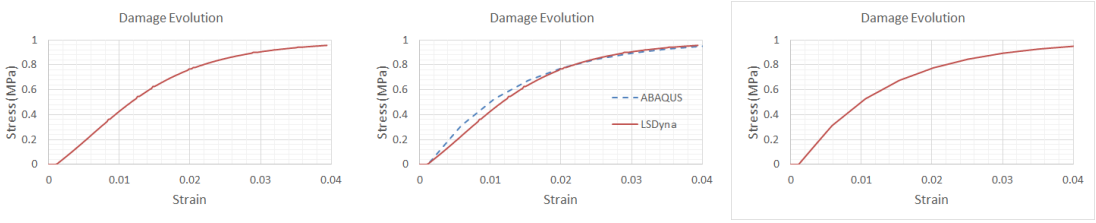

Figure 3: Compressive Damage evolution trend as of LS-DYNA (Left), Abaqus (Right) and their comparison (Middle).

The results of figs. 1-3 show that the models can be compatible with each other and give the same results in the case of uniaxial compression if the aim is to achieve identical stress vs. strain response in addition to observe same damage values and its corresponding plastic strain. However, it is clearly shown that lateral strains are not equal to each other in these two models. Because of using associate flow rule in material 159, it is expected to observe higher value of lateral expansion in this material which has been confirmed with the analysis results. The following figures are behavior of two material models under uniaxial tension:

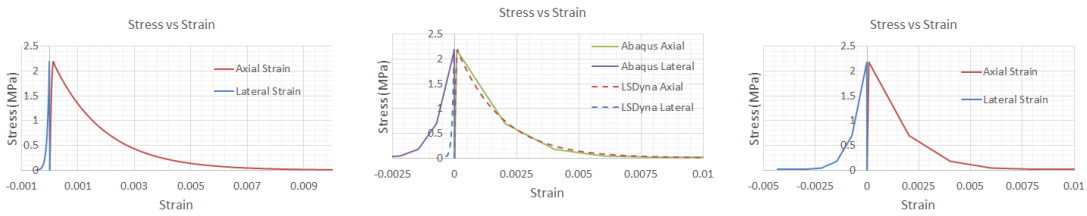

Figure 4: Uniaxial tension results of LS-DYNA (Left), Abaqus (Right), and their stress vs strain comparison (Middle).

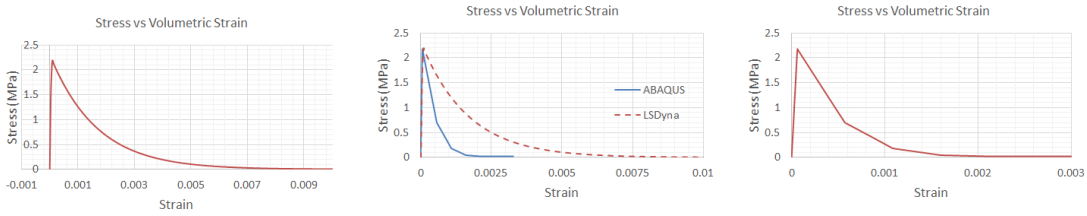

Figure 5: Extension to compaction behavior (there is not any!) as of LS-DYNA (Left), Abaqus (Right) and their comparison (Middle).

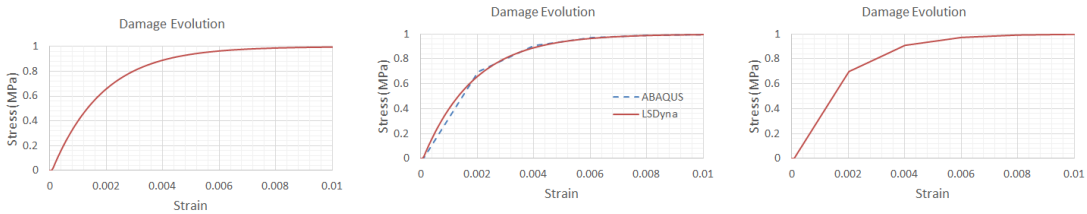

Figure 6: Tensile Damage evolution trend as of LS-DYNA (Left), Abaqus (Right) and their comparison (Middle).

After parameter matching of two material models in uniaxial tension and compression, some modelings have been done and comparisons are made for different load cases and the difference between response of material models has been discussed. The main focus of this section is on triaxial expansion vs triaxial compression behavior which are called CTE, CTC. The load path of CTE and CTC in $I_1 - J_2$ space is similar to each other but the direction is opposite ton each other. both are moving along the I_1 axis direction but CTE is moving towards most tensile point and CTC moves towards the most compressive point. The results of CTE has been shown in figures 7,8. Based on triaxial confined loading scenario, a tremendous increasing of

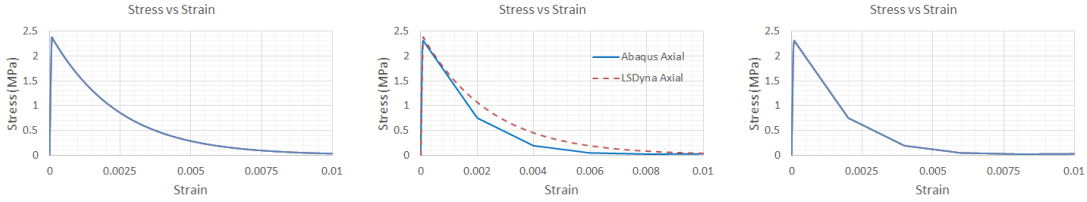

Figure 7: CTE results of LS-DYNA (Left), Abaqus (Right), and their stress vs strain comparison (Middle).

compressive strength has been observed in both models as show in fig. 9. In fact, according to expectation, no plastification has been observed in CDP model, which is based on an uncapped version of Drucker-Prager like behavior. Plastification has been observed in material 159 but like CDP, no damage was observed in the material.

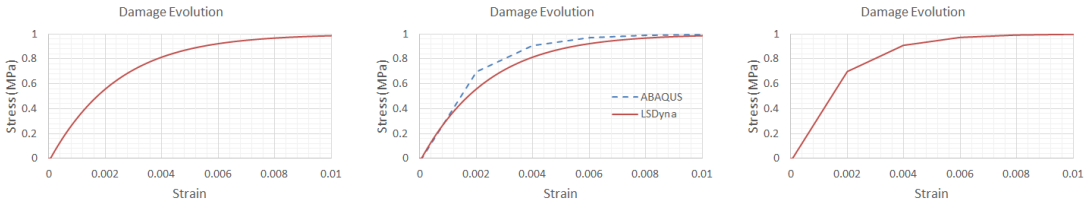

Figure 8: Tensile Damage evolution trend under CTE in LS-DYNA (Left), Abaqus (Right) and their comparison (Middle).

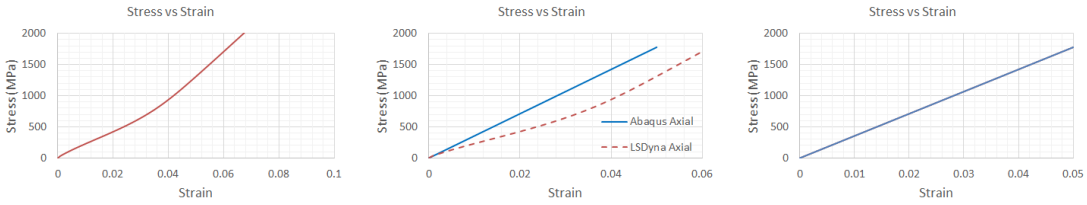

Figure 9: CTC results of LS-DYNA (Left), Abaqus (Right), and their stress vs strain comparison (Middle).

The results of compression under equibiaxial constant confining pressure for two material models have been obtained and compared in figures 10-12. As an example of higher level

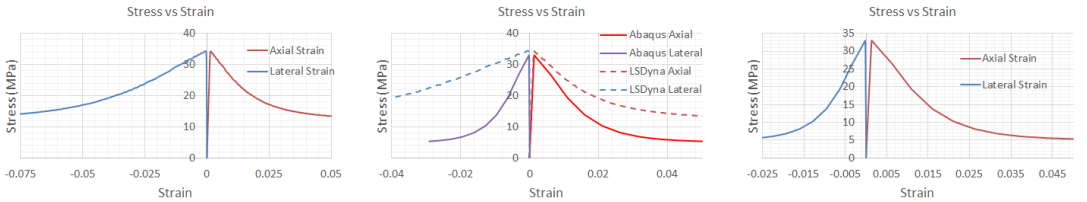

Figure 10: Results of low confinement pressure ($\sigma_{conf} = 1MPa$) with LS-DYNA (Left), Abaqus (Right), and their stress vs strain comparison (Middle).

of confinement, some modelings have been done when the model undergoes an equibiaxial confinement of $\frac{1}{2}f'_c$ prior to loading in he main axial direction. the results and comparisons are illustrated in figures 13-15. It can be observed from fig. 13 that the prediction of two models from biaxial behavior is different from each other while they are calibrated to each other in case of uniaxial loading condition. Since for both models, the shear is defined as an straight line, a parameter cannot be defined in order to match behavior of both models in three cases of loading (uni tension, uni compression and compression under low level of confinement). By looking at fig. 14, we can understand that even in the case of moderate confinements, a compaction to dilation behavior happens in material 159, while the behavior of CDP model is only compaction regime. It indicates the importance of considering non-associaticity in realistic modeling of material behavior. Being able to choose dilation angle, gives constitutive model the ability of performing more realistic and more complex modelings. It is also observed that in the higher levels of confinement, level of damage in models which associate damage with strength degradation is lower than the decoupled models due to lower amount of softening in material behavior.

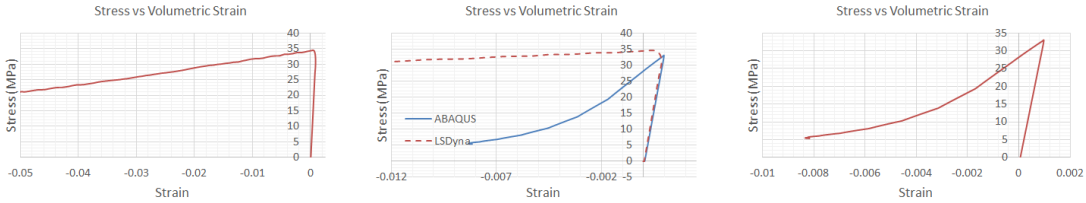

Figure 11: Compaction to Extension behavior (low confinement pressure $(\sigma_{conf} = 1MPa)$) as of LS-DYNA (Left), Abaqus (Right) and their comparison (Middle).

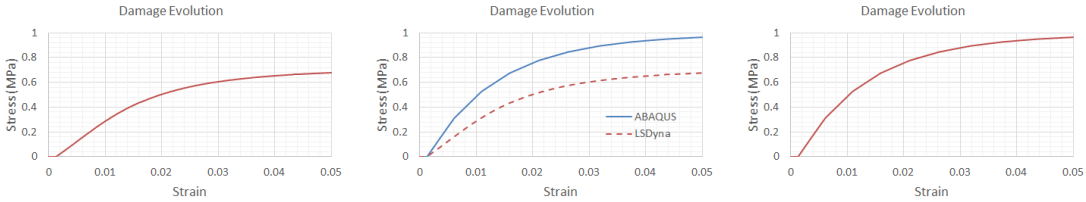

Figure 12: Compressive Damage evolution trend under low confinement pressure in LS-DYNA (Left), Abaqus (Right) and their comparison (Middle).

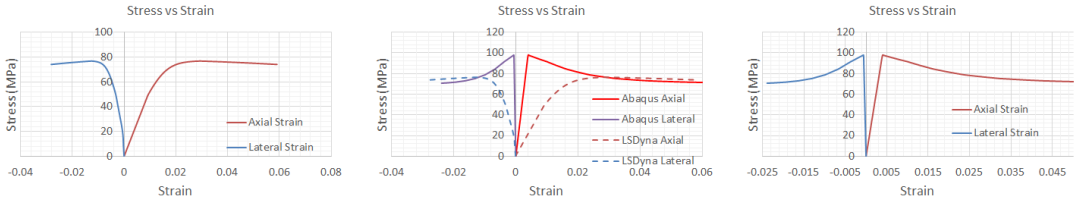

Figure 13: Stress vs. axial strain results for high confinement $(\frac{1}{2}f'_c)$ of LS-DYNA (Left), Abaqus (Right), and their stress vs strain comparison (Middle).

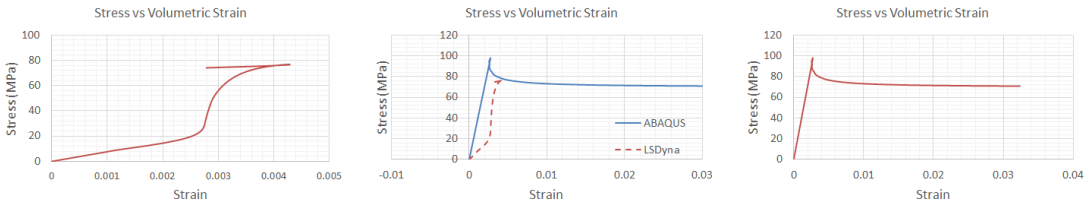

Figure 14: Compaction to Extension behavior (under high confinement $(\frac{1}{2}f'_c)$) as of LS-DYNA (Left), Abaqus (Right) and their comparison (Middle).

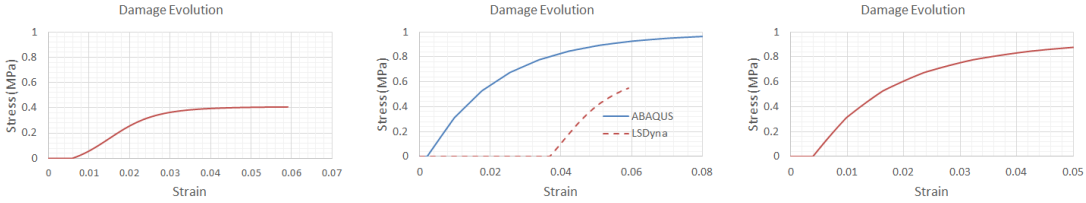

Figure 15: Compressive Damage evolution trend under high confinement $(\frac{1}{2}f'_c)$ in LS-DYNA (Left), Abaqus (Right) and their comparison (Middle).

Table 1: The material 159 parameters which are used to calibrate with CDP model

α	β_0	λ	θ	α_1	β_1	λ_1	θ_1
14.2	0.01929	10.51	0.2965	0.7473	7.25e-2	0.17	1.204e-3
α_2	β_2	λ_2	θ_2	f'_c	Aggregate size	G	K
0.66	7.25e-2	0.16	1.45e-3	28	16	1.15×10^4	1.26×10^4
R	X_0	D_1	D_2	W	G_c	G_T	G_s
5	90	2.5×10^{-4}	3.5×10^{-7}	0.05	10	0.1	0.1
B_1	B_2	B_3	B_4	D_1	D_2	D_3	D_4
500	100	50	10	0.05	0.1	1	10

Table 2: The CDP parameters

a_c	b_c	d_c	f'_c
0.8	110	75	28
a_t	b_t	d_t	f_t
0.4	700	600	2.2

5 Conclusions and Remarks

This paper has critically looked at two well known concrete material models (Lee-Fenves, Duvaut-Lion) which are implemented in two most widely used FEA software packages among researchers (ABAQUS, LS-DYNA, respectively) from a practical point of view to give general insights into modeling strategies to help reader choose a proper material model based on abilities and limitations of each model by emphasizing on difference between response of these material models under more complex loading paths, while their response under simple loading histories are identical to each other by choosing proper parameters. The models have been compared to each other initially under uniaxial compression and tension and after calibrating parameter values together, response of models in the cases of CTE, CTC and confined compression under low and high confining pressure has been obtained and compared to each other.

It has been observed that even in the case of uniaxial compression, there is a difference in dilatant behavior of models. The reason for that is CDP model uses a non-associate flow rule which can control the dilatation of response, while material 159 uses associate flow rule and it has been observe clearly that the volumetric strain is higher under associate flow condition which might not be a realistic response.

Under CTE condition, since both models are using a linear function for frictional area in $(I_1 - J_2)$ space, it is clear that none of the models are able to incorporate tiraxial extension strength as an independent material parameter. It can be solved by choosing a hyperbolic regime for shear regime that is asymptotic to linear curve in by moving towards compressive region in $(I_1 - J_2)$ space.

The behavior of two models in CTC conditions shows that proper cap behavior of CDP model can avoid linear elastic behavior in very high stress values. In addition, since for both material behaviors, the value of damage remains zero, which requires further analysis to find out how realistic is this value. It can be concluded from the confined load cases that under this condition, the peak value that both material models are giving has a small difference in addition to

dramatically different behavior in transition from compaction to expansion behavior in all cases of compressive loading.

REFERENCES

[1] K. Hibbitt and Sorensen, *ABAQUS/CAE User's Manual*. Hibbitt, Karlsson & Sorensen, Incorporated, 2002.

[2] L. Manual *Livermore Software Technology Corporation*, vol. 1, 2007. cited By 1.

[3] J. Lee and G. Fenves, "Plastic-damage model for cyclic loading of concrete structures," *Journal of Engineering Mechanics*, vol. 124, no. 8, pp. 892–900, 1998. cited By 739.

[4] J. Lubliner, J. Oliver, S. Oller, and E. Oate, "A plastic-damage model for concrete," *International Journal of Solids and Structures*, vol. 25, no. 3, pp. 299–326, 1989. cited By 729.

[5] T. Jankowiak and T. Lodygowski, "Identification of parameters of concrete damage plasticity constitutive model," *Foundations of civil and environmental engineering*, vol. 6, no. 1, pp. 53–69, 2005.

[6] S. V. Chaudhari and M. A. Chakrabarti, "Article: Modeling of concrete for nonlinear analysis using finite element code abaqus," *International Journal of Computer Applications*, vol. 44, pp. 14–18, April 2012. Full text available.

[7] M. R. Mousavi and A. Khaloo, "Effect of steel plate jacketing of columns in seismic behavior of concrete beam-column connections," in *6th National Congress on Civil Engineering*, 2011.

[8] G. Xotta, S. Beizaee, and K. Willam, "Localization analysis of coupled plasticity and damage models for dissipative materials," *Computational Modelling of Concrete Structures*, p. 439, 2014.

[9] R. M. Brannon and S. Leelavanichkul, "Survey of four damage models for concrete,"

[10] L. Malvar, J. Crawford, J. Wesevich, and D. Simons, "A plasticity concrete material model for dyna3d," *International Journal of Impact Engineering*, vol. 19, no. 9-10, pp. 847–873, 1997. cited By 245.

[11] H. Hansson and P. Skoglund, "Simulation of concrete penetration in 2d and 3d with the rht material model," *Swedish Defense Research Agency*, 2002.

[12] T. Borrvall and W. Riedel, "The rht concrete model in ls-dyna," in *Preceedings of the 8 th European LS-DYNA Users Conference, Strasbourg*, 2011.

[13] A. Fossum, R. Brannon, A. F. Fossum, and R. M. Brannon, "The sandia geomodel: theory and users guide," 2004.

[14] Y. D. Murray, "Users manual for ls-dyna concrete material model 159," tech. rep., 2007.

[15] M. D. Champiri, A. Attar, M. Hanifehzadeh, K. Willam, and B. Gencturk, "Long-term performance of dry storage structures," in *CONCREEP 10*, pp. 1593–1602.

[16] M. D. Champiri, A. Attar, M. Hanifehzadeh, K. Willam, and B. Gencturk, "Tipover simulation of degraded dry cask storage structures," in *Proceedings of the ASME 2015 International Mechanical Engineering Congress & Exposition -IMECE15*, ASME (Manuscript accepted for publication).

[17] J. Simo, J. Kennedy, and S. Govindjee, "Non-smooth multisurface plasticity and viscoplasticity. loading/unloading conditions and numerical algorithms," *International Journal for Numerical Methods in Engineering*, vol. 26, no. 10, pp. 2161–2185, 1988.

[18] H. Kupfer, H. K. Hilsdorf, and H. Rusch, "Behavior of concrete under biaxial stresses," in *Journal Proceedings*, vol. 66, pp. 656–666, 1969.

[19] G. Yang, M. Zomorodian, A. Belarbi, and A. Ayoub, "Uniaxial tensile stress-strain relationships of rc elements strengthened with frp sheets," *Journal of Composites for Construction*, p. 04015075, 2015.

[20] K. Willam, A. Mohammadipour, R. Mousavi, and A. S. Ayoub, "Failure of unreinforced masonry under compression," *Proceedings of the Structures Congress*, pp. 2949–2961, 2013.

[21] G. Xotta, S. Beizaee, and K. Willam, "Bifurcation investigations of coupled damage-plasticity models for concrete materials," *Computer Methods in Applied Mechanics and Engineering*, vol. 298, pp. 428–452, 2016.

[22] S. Beizaee, G. Xotta, and K. Willam, "Perforation studies on flat bars for xfem-based failure analysis," *Engineering Fracture Mechanics*, 2016.

[23] M. D. Champiri, S. H. Mousavizadegan, and F. Moodi, "A decision support system for diagnosis of distress cause and repair in marine concrete structures," *Computers & Concrete*, vol. 9, no. 2, pp. 99–118, 2012.

[24] M. D. Champiri, S. H. Mousavizadegan, and F. Moodi, "A fuzzy classification system for evaluating the health condition of marine concrete structures," *Journal of Advanced Concrete Technology*, vol. 10, no. 3, pp. 95–109, 2012.

[25] M. Rubin, "Simple, convenient isotropic failure surface," *Journal of engineering mechanics*, vol. 117, no. 2, pp. 348–369, 1991.